

Synthesis And Characterization of CdS/CeO₂ Nanocomposite With Improved Visible-Light Photocatalytic Degradation of Methyl Orange Dye

Tigabu Mekonnen Bekele (✉ tgbekele19@gmail.com)

Mekdela Amba University

Nano Express

Keywords: Nanotechnology, Degradation, Photocatalyst, AOPs, Nanoparticle, Ceria

Posted Date: July 23rd, 2021

DOI: <https://doi.org/10.21203/rs.3.rs-680076/v1>

License:   This work is licensed under a Creative Commons Attribution 4.0 International License.

[Read Full License](#)

Abstract

In this work, different types of photocatalysts in single (CdS and CeO₂) and binary (CdS/CeO₂ in different molar ratio: 0.5:1, 1:1 and 1:0.5) systems were synthesized by co-precipitation method. Crystal structure, surface area, morphology, band gap energy, functional groups and optical properties of the as-synthesized photocatalysts were characterized by using XRD, BET, SEM-EDX, UV/Vis, FTIR and PL instruments, respectively. Photocatalytic activities of single and binary nanocomposite were evaluated by using aqueous solution of model pollutant methyl orange dye (MeO). Photocatalytic activities of binary CdS/CeO₂ (1:1) nanocomposite were found to be higher than those of single counterparts. The photodegradation efficiencies of the binary system were found to be 53.73%. The reusability of binary photocatalyst was tested and only about 33% decrement was observed after four successive runs. Photocatalytic degradation of MeO dye follows the pseudo first order kinetics for the entire as-synthesized nanocomposite. The results also suggest that in the CdS/CeO₂ (1:1) nanocomposite the photoinduced electrons and holes can be effectively separated.

Introduction

Nature is contaminated by especially wastewater effluents of industrial manufacturing companies contain toxic organic compounds [1]. Dyes are a well-known source of environmental pollution and therefore their removal from waste water receives increasing attention. They are generally resistant to light, water, oxidizing agents and many chemicals and therefore difficult to degrade once released into the aquatic systems. Azo dyes are the largest and most versatile class of organic dye-stuffs. These contain one or more azo bonds (–N = N–) as a chromophore group in association with aromatic structures containing functional groups such as –OH and –SO₃H. The complex aromatic structures of azo dyes make them more stable and more difficult to remove from the effluents discharged into the water bodies [2]. A number of physical, chemical and biological techniques had been reported for the treatment of all types of dyes with limited success.

Recently, many processes have been extensively applied for the treatment of dye containing wastewater such as: incineration, biological treatment, ozonation and adsorption on solid phase. However, these procedures have their own limitations. These is why the most advanced technique which is called advanced oxidation processes (AOPs) have been developed during the last decade since they are able to deal with the problem of dye destruction in aqueous systems.

AOPs were based on the generation of very reactive species such as hydroxyl radicals (·OH) that oxidize a broad range of pollutants quickly and non-selectively [3]. AOPs such as plasma oxidation, ozonation, Fenton, photo-Fenton catalytic reactions H₂O₂/UV processes and semiconductor mediated photocatalysis have been studied under a broad range of experimental conditions in order to reduce the color and organic load of dye containing effluent waste waters [4, 5].

The most important among those advanced oxidation processes is called heterogeneous photocatalytic oxidation which is often referred to as photocatalysis. This method deals with the oxidation mostly of organic molecules and compounds by means of solid metal oxide semiconductor as catalyst, which is activated by the incidence of radiation of an appropriate wavelength. It can take place both in the aqueous phase as well as in the gas phase. Among AOPs, heterogeneous photocatalysis appears as the most emerging destructive technology. Chemical treatment of wastewaters by AOPs can result in the complete mineralization of the pollutants to simple harmless end products such as carbon dioxide, water and inorganic salts. Ideally, a semiconductor photocatalyst for the purification of water should be chemically and biologically inert, photocatalitically active, easy to produce and use, and activated by UV or sunlight [6].

Semiconductor-based photocatalysis is a promising avenue to solve the worldwide energy shortage and environmental pollution using the abundant solar light [7]. Of the well-known photocatalysts, cerium dioxide (CeO_2), as a fascinating rare earth material, has attracted much attention owing to its high activity, low cost and environmentally friendly properties [8]. It shows promising photoactivity for the degradation of organic pollutants and water splitting for hydrogen generation. Nevertheless, pristine CeO_2 can only be excited by ultraviolet light (UV) because of its wide band gap (about 3.2 eV), limiting its further application in the visible light region. In order to highly utilize solar energy, various methods, such as doping, noble metal deposition and forming composites have been designed to enhance the absorption of CeO_2 photocatalysts in the visible light region. Among them, the most effective strategy is the coupling of two semiconductors, CeO_2 and another semiconductor, to form a composite [9].

There are many reports available on mixed metal oxides of CeO_2 to improve its thermal stability and increase its photocatalytic performance [10]. Nanocomposites such as TiO_2 - CeO_2 [11], CeO_2 - ZnO [12], ZrO_2 - CeO_2 [13] and $\text{Ag}_3\text{PO}_4/\text{CeO}_2$ [14] have been prepared and their photocatalytic activities under visible irradiation investigated.

However, the prepared binary photocatalysts have moderate photocatalytic activity under visible-light illumination. In this research, we hypothesized a good photocatalytic activity as the result of binary CdS/CeO_2 n-n heterostructured nanocomposite. CdS could be able to form "A-type" heterojunction with CeO_2 given the more negative potential expected to be effective in exploiting both e^- and h^+ in the redox process [15]. In this work, the principal objective is to synthesize binary CdS/CeO_2 and evaluates the photocatalytic activity of the as-synthesized nanocomposite for the degradation of model pollutant dye, Methyl orange (MeO).

Experimental

2.1. Chemicals

Cerium nitrate hexahydrate $\text{Ce}(\text{NO}_3)_3 \cdot 6\text{H}_2\text{O}$ and ammonia solution (25% Loba chemicals Ltd, India), cadmium acetate tetrahydrate $(\text{Cd}(\text{CH}_3\text{COO})_2 \cdot 4\text{H}_2\text{O})$ and di-sodium sulfide $(\text{Na}_2\text{S} \cdot 9\text{H}_2\text{O})$ were used as the precursors of CeO_2 and CdS , respectively. All chemicals were analytical grade and are bought from Sigma Aldrich.

2.2. Synthesis of Photocatalysts

2.2.1. Synthesis of CeO_2 Nanoparticle

Cerium oxide nanoparticle was prepared by precipitation method [16]. An aqueous solution of 0.1 M of cerium nitrate hexahydrate $\text{Ce}(\text{NO}_3)_3 \cdot 6\text{H}_2\text{O}$ in deionized water was prepared and stirred for 30 min. The clear solution was precipitated by dropwise addition of aqueous NH_4OH solution with continuous stirring until precipitation gets completed. The stirring was continued for another 2 h and the reaction condition then maintained at $\text{pH} = 8$. The reaction mixture was then stirred for 12 h to complete the precipitation process. Ash color solution changed into yellow solution after an hour of stirring time. The mixture was aged for 12 h. The resulting yellow colored slurry was decanted, filtered and washed several times with deionized water and ethanol. The precipitate was oven dried at $140\text{ }^\circ\text{C}$ for 12 h and calcined at $500\text{ }^\circ\text{C}$ for 3 h to promote the crystallization [17].

2.2.2. Synthesis of CdS Nanoparticle

In this study, we have used cadmium acetate tetrahydrate $(\text{Cd}(\text{CH}_3\text{COO})_2 \cdot 4\text{H}_2\text{O})$ as a Cd^{+2} ion source and di-sodium sulfide nanohydrate $(\text{Na}_2\text{S} \cdot 9\text{H}_2\text{O})$ as S^{-2} ion source, respectively. For the synthesis of CdS nanoparticle using precipitation method, equal molarity of (0.1 M) $\text{Cd}(\text{CH}_3\text{COO})_2 \cdot 4\text{H}_2\text{O}$ and $\text{Na}_2\text{S} \cdot 9\text{H}_2\text{O}$ solution were prepared in separate beakers. Then sodium sulfide solution was added dropwisely through continuous stirring for 2 h at room temperature to form a clear solution. During the reaction N_2 gas was continuously purged through the suspension. Then the yellow precipitate was collected by centrifugation and washed three times with deionized water and ethanol to remove the residue. Finally, the obtained CdS nanoparticle was further dried at $70\text{ }^\circ\text{C}$ for 5 h. The clean solid precipitate was calcined at $300\text{ }^\circ\text{C}$ for 2 h in a furnace, ground into powder and kept in a container [18].

2.2.3. Synthesis of CdS/CeO_2 Nanocomposite

In a typical procedure, 0.1 M of the as-synthesized CeO_2 powder were dispersed in 100 mL of distilled water and sonicated for 30 min, then 0.1 M of $\text{Cd}(\text{CH}_3\text{COO})_2 \cdot 4\text{H}_2\text{O}$ was added. After 1 h of stirring, equal molarity of $\text{Na}_2\text{S} \cdot 9\text{H}_2\text{O}$ solution was added dropwisely into the mixed solution. The precipitate was filtered and washed with distilled water and ethanol several times, and then dried in an oven at $60\text{ }^\circ\text{C}$ for 24 h to obtain CdS/CeO_2 nanocomposite [19]. The CdS/CeO_2 nanocomposite was done in four molar ratios (0.5:1, 1:1 and 1:0.5) of $\text{CdS}:\text{CeO}_2$. The obtained powder was then ground to get fine particles.

2.3. Characterization of the As-synthesized Photocatalysts

2.3.1. X-ray Diffraction (XRD) Study

The structures of all the as-synthesized photocatalyst were examined by XRD at room temperature at step scan rate of 0.02° (step time: 1s; 2θ range: $5.0-90.4^\circ$), which is equipped with an X-ray source of a CuK α radiation (wavelength of 0.15406 nm) using 45 kV accelerating voltage and 40 mA applied current. Finally, XRD patterns were collected with X'Pert Pro PANalytical.

2.3.2. Determination of Surface Area

The specific surface area of each of the as-synthesized photocatalyst were calculated from the N₂ adsorption-desorption isotherm at liquid-nitrogen temperature - 196 °C (77 K) and the micropore surface area were calculated by using the Brunauer-Emmett-Teller (BET) method.

2.3.3. SEM-EDX Study

Solid morphologies and particle distribution of the as-synthesized photocatalyst were determined by scanning electron micrographs (SEM Hitachi TM1000 with EDX detector) with a backscattered detector instrument; a gold film was sputtered into the sample prior to observation. From energy dispersive X-ray [EDX, an acquisition time (s) 40.0; process time 3 h; and an accelerating voltage (kV) 15.0] link with SEM the elemental percent weight distribution of the as-synthesized sample was determined.

2.3.4. UV/Vis Diffuse Reflectance Study

The optical absorption spectra and band gaps of the as-synthesized photocatalysts were determined using UV/Vis spectrophotometer. The solid state absorbance of the photocatalyst was measured by scanning over the wavelength range of 200–900 nm.

2.3.5. FTIR Study

The as-synthesized photocatalyst was characterized using FTIR (Spectrum 65, PerkinElmer) instrument. Dry mass of the photocatalyst was thoroughly mixed with a given dry mass of KBr and ground to a fine powder. A transparent disc was formed by applying a pressure in moisture free atmosphere. The IR absorption spectrum was recorded between 400 and 4000 cm^{-1} .

2.3.6. Photoluminescence (PL) Study

Photoluminescence (PL) spectra were measured at Haramaya University using RF 5301PC Shimadzu photoluminescence. The spectra were obtained in the range of 250–650 nm.

2.4. Photocatalytic Degradation Studies

Photocatalytic activities of the entire as-synthesized sample were tested for the degradation of aqueous solution of methyl orange (MeO) dye. For example in typical photocatalytic experiment, 10 ppm of MeO was mixed with 0.2 g/L of the photocatalyst. The mixture was magnetically stirred for 1 h in the dark to ensure adsorption/desorption equilibrium. Then the suspension was irradiated with visible light irradiation with continuous stirring using magnetic stirrer and the absorbance was measured in 20 min

time interval to monitor the reaction of MeO aqueous solution degradation. The distance between the light source and the dye solution is 20 cm. During the process air/oxygen was purged in to the solution using pipette. Then 10 mL suspension was withdrawn at 20 min time interval and centrifuged at 3000 rpm for 10 min. Dye absorbance was determined using UV/Visible spectrophotometer at the λ_{max} of MeO solution. Percent degradation (%) was calculated using the following equation [20].

$$\% \text{ Degradation} = \frac{C_0 - C_t}{C_0} \times 100 \quad (1)$$

When the concentration is very low, the observed rate constant, k_{obs} (min^{-1}) was determined from the simplified Langmuir-Hinshelwood model as given below [21]:

$$\text{Rate} = \ln(C_t/C_0) = -kt \quad (2)$$

Where k_{obs} is the observed rate constant in min^{-1} , C_t is the absorbance at a given time, C_0 is the absorbance at initial time and t (min) is the reaction time. Hence, the linear fit between C_t/C_0 and irradiation time demonstrates the photocatalytic degradation rate. A higher k_{obs} value indicates a better photocatalytic activity of an investigated sample.

2.5. Stability Test of the As-synthesized Photocatalyst

The recycling of the photocatalyst was performed as follows [22]: after a first photodegradation cycle of a 10 ppm solution of methyl orange (MeO) dye using 0.15 g/L of the as-synthesized photocatalyst and 160 min irradiation time, the treated solution of the dye was centrifuged for 10 min to settle the catalyst. The liquid phase was filtered and then the solid phase containing the photocatalyst was carefully separated for reuse. The recovered photocatalyst was washed by sufficient amount of deionized water and ethanol. Finally, the photocatalyst was dried in an oven for 12 h at 100 °C before the use for next catalytic cycle and then reintroduced into fresh cycle. The process was repeated four times. The 10 mL suspension was withdrawn at 20 min time interval and centrifuged at 3000 rpm for 10 min. The MeO degradation and photocatalytic stability of as-synthesized photocatalyst layer was measured at the end of each cycle.

Results And Discussion

3.1. Characterization of the As-synthesized Photocatalysts

3.1.1. XRD Analysis

X-ray diffraction is the most powerful and successful technique commonly used for determining the structure of crystals and the arrangement of atoms within a crystal [23]. The characteristic peaks on the XRD patterns of the as-synthesized photocatalyst: CeO_2 , CdS and CdS/ CeO_2 were shown in Fig. 1.

Accordingly, diffraction peaks observed at scattering angle observed at 2θ of 28.52, 33.19, 47.38, 56.54, 59.09, 70.01, 76.78, 78.99 and 88.24° corresponding to (111), (200), (202), (311), (222), (400), (313), (402) and (422) lattice plane respectively represents the cubic fluorite structure of CeO₂ [24]. The broad peaks observed at 2θ of 25.02, 26.42, 28.19, 36.24, 43.55, 48.00, 52.02, 54.66, 67.03, 70.11, 71.34, 72.81, 76.03, 80.52 and 83.44° corresponding to (100), (002), (101), (012), (110), (013), (112), (044), (023), (210), (211), (114), (212), (300) and (213) crystal plane can be ascribed to the hexagonal greenockite structure of CdS nanoparticle [25, 26]. The broadening of the diffraction peak indicates the nanocrystalline nature of the samples and provides information about crystallite size. As the width increases, the particle size decreases and vice versa [27].

In the case of CdS/CeO₂ binary system, most of the diffraction peaks observed could be ascribed to cubic fluorite structure of CeO₂ nanoparticle. However, diffraction peaks at 2θ values of 26.82, 44.01 and 52.21° indicate the presence of hexagonal greenockite structure of CdS in the binary system [15, 19]. No other phases can be observed in the XRD patterns of CdS/CeO₂ nanocomposite, suggesting that no impurity exists in the sample. It is found that the diffraction peaks for both CeO₂ and CdS can be observed from the XRD pattern of the composite, indicating the formation of CdS/CeO₂ composite. The absence of other peaks in the XRD pattern of core/shell composite implies that it only consists of CeO₂ and CdS.

The average crystallite size of each of the as-synthesized photocatalyst was calculated using the Debye-Scherrer formula [28];

$$D = \frac{K\lambda}{\beta \cos\theta} \quad (3)$$

Where, D = crystallite size in nm, K = the shape factor constant taken as 0.9; β is the full width at half maximum (FWHM) in radians, λ is the wavelength of the X-ray (0.15406 nm) for Cu target K α 1 radiation and θ is the Bragg's angle. Generally the calculated average crystalline size of the as-synthesized photocatalyst confirms the involvement of good crystalline nano range between 10 and 50 nm [29] as summarized in Table 1.

Table 1
Crystal size of the as-synthesized photocatalysts

Photocatalyst	2θ (degree)	β (radians)	D (nm)
CeO ₂	28.52	0.02804	18.406
CdS	43.55	0.02338	23.576
CdS/CeO ₂ (1:1)	28.61	0.01004	47.992

3.1.2. Determination of Surface Area (BET)

Surface area of the as-synthesized nanocomposite was determined by the Brunauer-Emmett-Teller (BET) method. Table 2 shows the specific surface area of each sample investigated by nitrogen adsorption-desorption isotherm analysis. The specific surface area is largest for CeO₂ (77 m²g⁻¹) whereas lowest for Ag₃PO₄ (0.122 m²g⁻¹) showing the compacted nature of the later.

As indicated in Table 2, the specific surface area can be calculated and those of single and binary nanocomposite which is about 43.8627, 44.3277, 43.5162, 17.4935 and 37.6739 m²g⁻¹ for the obtained CdS/CeO₂ (1:0.5), CdS/CeO₂ (1:1), CdS/CeO₂ (0.5:1), CdS and CeO₂ samples, respectively. The CdS/CeO₂ (1:1) composite has the largest specific surface area may be because the modification of CeO₂ can increase the dispersion of the CdS nanoparticle, as well as because the CeO₂ nanoparticles have relatively large surface area. It is expected that this can facilitate enhancing adsorption of reactant molecules and, thereby, the enhanced photocatalytic activity [30].

Table 2
Specific surface area of the as-synthesized photocatalysts

As-synthesized photocatalyst	BET surface area (m ² g ⁻¹)
CeO ₂	37.6739 ± 0.1923
CdS	17.4935 ± 0.0745
CdS/CeO ₂ (1:0.5)	43.8627 ± 0.7335
CdS/CeO ₂ (1:1)	44.3277 ± 0.0012
CdS/CeO ₂ (0.5:1)	43.5162 ± 0.1108

3.1.3. SEM-EDX Image Study

Morphological images of the as-synthesized photocatalysts; CeO₂, CdS and CdS/CeO₂ were investigated as shown in Fig. 2a-c respectively.

The EDX spectrum shows the presence of all the relevant components in each photocatalyst. According to the SEM images shown in Fig. 2a, the morphology of CeO₂ nanoparticle is observed to be nearly spherical with slight agglomeration (single phase). From the SEM image shown in Fig. 2b it is noticed that the surface morphologies are in the form of assemblies of CdS nanoparticles and uniformly distributed over the entire surface. The EDX spectrum and elemental mapping shows that the CdS nanoparticle contains average stoichiometric composition with 80.45% of cadmium and 19.55% of sulphur. As can be seen from Fig. 2c, the CdS/CeO₂ composite also exhibited no distinct morphology, though cubic like structures appeared rarely. On the other hand, the percent chemical distribution gradients across the surface of the sample (w/w %) were determined from results of energy dispersive X-ray (EDX) analysis. Elemental composition (weight %) of the CdS/CeO₂ photocatalysts contains average stoichiometric composition with 24.85% of cerium, 62.5% of cadmium and 12% of sulphur. Interestingly,

EDX spectrum result exhibits the presence of Ce, Cd and S peaks indicating the CeO₂ and CdS nanoparticles [17].

3.1.4. UV/Vis Diffuse Absorption Spectra of the As-synthesized Photocatalysts

UV/Vis diffuse absorption edges of the as-synthesized photocatalysts are obtained from plot of absorbance against wavelength.

The intercept of the tangent line on descending part of the absorption peak at the wavelength axis gives the value of diffuse absorption edge (nm). In such case band gap energy (E_g) of the as-synthesized photocatalysts was obtained from Eq. 4 [31].

$$E_g = \frac{1240 \text{ eV}}{\lambda_{\text{max}}} \quad (4)$$

Where, E_g is bandgap energy in electron volts and λ_{max} is wavelength (nm) corresponding to absorption edge.

But estimating the band gap using the above approach sometimes may not provide clear tangential line when the peak is not well resolved for the samples. To avoid the difficulties in obtaining band gap energy from UV/Vis absorption spectroscopy in dispersed samples, diffuse reflectance measurements of dry powders can be performed. The optical absorption properties of each of the as-synthesized photocatalyst were investigated by using a UV/Vis diffuse reflectance spectrometer in the range of 200–900 nm. The band gap values of the photocatalysts were determined by analyzing the optical data with the expression for the optical absorbance α and the photon energy hv using Tauc's plot [32, 33, 34].

$$\alpha hv = A (hv - E_g)^{n/2} \quad (5)$$

where α is the absorption coefficient, which is proportional to the absorbance, h is the Planck's constant (J.s), ν is the light frequency (s⁻¹), A is the absorption constant, E_g the band gap energy and n is a constant related to the electronic interband transition. n = 2 for an indirect allowed transition (plotted as (αhv)^{1/2} versus E_g), n = 3 for an indirect forbidden transition (plotted as (αhv)^{1/3} versus E_g), n = 1/2 for a direct allowed transition (plotted as (αhv)² versus E_g), n = 3/2 for a direct forbidden transition [plotted as (αhv)^{2/3} versus E_g] [35]. The band gaps was then determined by extrapolating the straight line portion of the (αhv)² versus (hv) graphs to the (hv) axis until (αhv)^{1/n} = 0 the linear section of this spectra as shown in the Fig. 3.

The absorption edges of the binary (CdS/CeO₂) photocatalysts are well extended to visible regions of spectrum as compared to the single nanoparticles.

This may be due to the effect of modification in the electronic levels of each single nanoparticle by making them binary composite.

Based on Tauc's plot as Eq. (5) the band gaps for all the as-synthesized materials were displayed in Table 3. The calculated band gaps of the single systems: CeO₂ and CdS are found to be 3.26 eV and 2.48 eV respectively. These findings are similar with previous reports made on these nanoparticles [17, 19, 36, 37]. The binary systems CdS/CeO₂ (molar ratio: 1:0.5, 1:1 and 0.5:1) have band gaps of 2.27 eV, 2.23 eV and 2.29 eV respectively. This finding also similar to previous reports made on the same nanoparticles [15, 17, 19].

Table 3
Maximum wavelength and band gap energy (E_g) of the as-synthesized photocatalysts

As-synthesized photocatalyst	Max. Wavelength	Band gap (E _g) eV
CeO ₂	380	3.26
CdS	500	2.48
CdS/CeO ₂ (1:0.5)	546	2.27
CdS/CeO ₂ (0.5:1)	542	2.29
CdS/CeO ₂ (1:1)	555	2.23

3.1.5. FTIR Study of the As-synthesized Photocatalysts

The FTIR spectrum in the mid-infrared region is the feature of a particular compound that gives the information about the functional groups, molecular geometry and intra/intermolecular interactions. Both inorganic and organic materials can be analyzed in the spectrum.

From the as-synthesized photocatalyst, the functional groups of CeO₂ were analyzed by FTIR in the range from 400 to 4000 cm⁻¹ and displayed in Fig. 4. In case of CeO₂, the band at 3435 and 1620 cm⁻¹ corresponds to the O-H stretching vibration and -OH scissor bending mode respectively, which is originated from physical absorbed (H-bonded) water molecules or surface -OH groups [38, 39]. The band located around 1047 cm⁻¹ has been attributed to the C-O stretching vibration may be from the additional CO₂ that was absorbed at CeO₂ surface [40]. The wide band at 1315 cm⁻¹ consists of the symmetrical stretching mode of N = O and the inside bending mode of N-H. The peak at 850 cm⁻¹ attributed to outside bending mode of N-H [41, 42].

The peaks observed at 1387 cm⁻¹ could be ascribed to the stretching vibration of N-O nitrate groups (NO₃⁻) which resulted from a precursor solution of Ce(NO₃)₃.6H₂O that was used to synthesis the nanoparticle (CeO₂) [43]. The intense band at 521 cm⁻¹ corresponds to the Ce-O stretching vibration [17, 44].

3.1.6. Photoluminescence (PL) Study of the As-synthesized Photocatalysts

PL is mainly used as a diagnostic and development tool in semiconductor research, since it can provide information about the electronic structure and the emission mechanism of the material [45]. The PL emission spectra of different photocatalysts (CeO_2 , CdS and CdS/ CeO_2 (in 0.5:1, 1:1 and 1:0.5 molar ratios)) were determined. The order of intensity is $\text{CeO}_2 > \text{CdS} > \text{CdS}/\text{CeO}_2$ (0.5:1) $> \text{CdS}/\text{CeO}_2$ (1:0.5) $> \text{CdS}/\text{CeO}_2$ (1:1) as indicated in the Fig. 5.

In binary nanocomposite the photoinduced electrons and holes can be effectively separated and hence excitation PL intensity goes down. This is because, lower the excitation PL intensity, stronger the capacity of coupled materials to capture photoinduced electrons, higher the separation rate of photoinduced electrons and holes, and higher the photocatalytic activity [46]. So, in this study it was clearly observed that the lower PL emission spectra were recorded for CdS/ CeO_2 (1:1) nanocomposite.

This might be also due to the photogenerated electron hole pair in CeO_2 separated well due to the synergy effect of coupling of A-type heterojunction (CdS/ CeO_2). In general the PL intensities of single systems were found to be higher than the binary system photocatalyst.

3.2. Photocatalytic Studies

3.2.1. Photocatalytic Activities of the As-synthesized Photocatalysts

Methyl orange (MeO), with a characteristic absorption at 464 nm is chosen as a typical organic pollutant for testing the photocatalytic activity of the as-prepared products. The photocatalytic activities of all the as-synthesized sample were evaluated by testing their ability in the degradation of MeO (initial dye concentration of 10 ppm and catalyst load of 0.2 g/L) under 160 min visible irradiation time. The degradation rate was analyzed by plotting C_t/C_0 versus irradiation time. The results show that the characteristic absorption peaks corresponding to MeO decrease rapidly as the exposure time increases, indicating the decomposition of MeO and the significant reduction in the MeO concentration.

The photocatalytic performance of CeO_2 , CdS and CdS/ CeO_2 (in 0.5:1, 1:1 and 1:0.5 molar ratios) photocatalyst was first evaluated by the degradation of model pollutant MeO under visible light irradiation. Before the photocatalytic reaction, an adsorption step in dark conditions was allowed to take place during 60 min. The result indicates that the adsorption capacity of binary and single photocatalyst become in the order of $\text{CeO}_2 < \text{CdS} < \text{CdS}/\text{CeO}_2$ (0.5:1) $< \text{CdS}/\text{CeO}_2$ (1:0.5) $< \text{CdS}/\text{CeO}_2$ (1:1). The photocatalytic activities of pure CeO_2 and CdS were lower than that of the composite photocatalyst. They decolorized 18.58, 27.07, 32.06, 35.98 and 53.73 % of MeO in 160 min of irradiation time respectively. The photocatalytic activities of pure CeO_2 are lower than CdS due to its higher band gap energy which makes it less sensitive to visible irradiation unlike other single counterparts [47].

The increment of photocatalytic degradation efficiency of CdS from that of CeO_2 over MeO solution is due to the efficient charge separation, narrow band gap that makes it sensitive to visible portion of the

spectrum, less electron-hole recombination, and a wide range of optical absorption of light by the composite could be possible reasons for the enhanced photoactivity [36]. In the A-type heterojunction system CdS/CeO₂ (1:1), the increased photocatalytic activities of CeO₂ could be initiated by conduction band electrons of CdS that involve in the photoreduction process [26].

There are many reports available on the photocatalytic degradation efficiency of binary nanocomposite (A-type) over different azo dyes (MeO). For A-type heterojunction, CdS/CeO₂, CdS/ZnO and CdS/TiO₂ also shows percent decolorization about 38.00, 49.30 and 55.00% over methyl orange dye respectively in different irradiation time [17, 48, 49]. In our case 53.73% for A-type heterojunction in 160 min irradiation time which is partially in line with the previous reports on both heterojunction.

The kinetics of the photocatalytic degradation was also exhibited using the pseudo-first-order reaction [50]. The rate constant of the binary CdS/CeO₂ (1:1) nanocomposite was higher than single and binary in other ratio photocatalysts, indicating the presence of a synergistic effect as indicated in Table 4. Among them, the apparent rate constants of CdS/CeO₂ (1:1) was the highest, calculated based on the equation $\ln(C_t/C_0)$ per irradiation time, and it was almost 18, 12, 8.9 and 6.13 times higher than that of CeO₂, CdS, CdS/CeO₂ (0.5:1) and CdS/CeO₂ (1:0.5) respectively.

Table 4
The apparent rate constants and % degradation of the as-synthesized photocatalysts after 160 min

As-synthesized photocatalyst	Degradation (%)	Rate constant, $k (\times 10^{-4} \text{ min}^{-1})$
CeO ₂	18.58	9.006
CdS	27.07	55.210
CdS/CeO ₂ (1:1)	53.73	162.11
CdS/CeO ₂ (0.5:1)	32.06	80.150
CdS/CeO ₂ (1:0.5)	35.98	108.072

3.3. Photocatalytic Stability of the As-synthesized Photocatalyst

In addition to photocatalytic efficiency, the stability of photocatalyst is also very important for practical application. To evaluate the stability of photocatalytic performance of binary CdS/CeO₂ (1:1), the circulating run in the photocatalytic degradation of MeO was carried out under visible light irradiation. The process was repeated up to four times. As exhibited in Fig. 7 the studies revealed that the composite demonstrated moderate stability after recovery.

In the first cycle 53.16% of the dye was degraded after 160 min of irradiation time. Subsequently the second, third and fourth cycle degraded 38.71, 23.17 and 17.41% of the dye corresponding to the rate constant (k) from 0.00493 to 0.00310, 0.00201 and 0.00120 min⁻¹ respectively. Agglomeration and sedimentation of the dye around the composite particles after each cycle of photocatalytic degradation is a possible cause of the observed decrease on the degradation rate, because each time the photocatalyst is reused new parts of the photocatalyst surface become unavailable for dye adsorption and thus photon absorption, reducing the efficiency of the catalytic reaction [51, 52]. Besides, one might expect a loss in the photocatalyst during recycling which eventually affect catalytic activity after each cycle.

This decreases the degradation rate of the as-synthesized photocatalyst may be due to the weakening of the absorbance ability of the catalyst or the loss of some catalyst during the cycling reaction. The result demonstrates that CdS/CeO₂ (1:1) nanocomposite shows a good photocatalytic performance as well as moderate stability after 4 cycles in 160 min.

3.4. General Proposed Mechanism of degradation of MeO Using CdS/CeO₂

According to the above experimental research, a probable mechanism of charge transfer and photocatalytic degradation of organic pollutant methyl orange (MeO) over the CdS/CeO₂ nanocomposite under visible light irradiation is put forward and illustrated in Fig. 8. The light illumination on CdS/CeO₂ nanocomposite causes the generation of electron (e⁻) in conduction band (CB) and holes (h⁺) in the valence band (VB).

Under visible light irradiation, the CdS can be activated, and the photoinduced electrons at the conduction band of CdS are transferred to the conduction band of CeO₂. The electrons will then react with water to produce hydrogen. On the other hand, the photoexcited holes at the valence band of CdS nanoparticles are captured by the MeO dye.

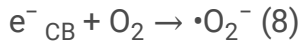
At CB site, molecular oxygen (O₂) forms superoxide radical •O₂⁻ in the presence of the photoexcited CB e⁻ and subsequently reacts with H⁺ to form HO₂• radical species. During the e⁻ transfer from CdS to CB of CeO₂, the generated photoinduced h⁺ in VB might react with water (H₂O) and the adsorbed MeO dye molecule to yield hydroxyl radical (•OH) and MeO•⁻ anions radical respectively [53]. On the other hand, electrons in the CeO₂ CB can migrate to its VB, while the holes generated in the CeO₂ VB move to CdS VB surface [54]. It is known that these oxygenous radicals (•O₂⁻, •OH and HO₂•) act as potential oxidizing and reducing species for the degradation of organic molecules (MeO) [55]. The proposed photoreaction mechanism of CdS/CeO₂ composite over MeO degradation under visible light follows:



Oxidative reaction



Reductive reaction



Generally:



In our case, on comparison with single and binary photocatalysts, the superior photocatalytic activity of binary nanocomposite under visible light might result from the enhanced charge separation and the formation of more active radicals ($\cdot O_2^-$ and $\cdot OH$) which are induced by the synergetic effect between CdS and CeO_2 . As a result, CdS/ CeO_2 nanocomposite delivers high photogenerated e^- - h^+ pair charge separation and produces sufficiently high amount of radicals for the high degradation of MeO dye under visible light irradiation. The photocatalytic performance of the photocatalyst mainly depends on: (i) its light absorption properties; (ii) the rates of reduction and oxidation on the surface of the catalyst by the electrons and holes; and (iii) the electron-hole recombination rate [56].

Declarations

Declaration of Competing Interest

This manuscript entitled with "Synthesis and Characterization of CdS/ CeO_2 Nanocomposite with Improved Visible-Light Photocatalytic Degradation of Methyl Orange Dye" consists of 3 tables and 8 figures. It has not been published previously; it is not under consideration for publication elsewhere. If accepted, it will not be published elsewhere in the same form, in English or in any other language.

References

1. Akpan, U. and Hameed, B. 2009. Parameters affecting the photocatalytic degradation of dyes using TiO_2 based photocatalysts. *Journal of Hazardous Materials*, 170: 520-529.
2. Jalil, A.A., Adam, S.H., Rahim, N.D., Arif, M., Aziz, A., Hanis, N., Hairom, H. and Khairul, N.M. 2010. Adsorption of methyl orange from aqueous solution onto calcined Lapindo volcanic mud. *Journal of Hazardous Materials*, 181: 755-762.
3. Sharma, V., Kakodia, A., Sharma, B., Pamecha, S. and Khandelwal, R. 2013. Photocatalytic degradation of Brilliant Blue-R by ZnO in aqueous media. *International Journal of Green and Herbal*

Chemistry, 2(3): 730-736.

4. Kansal, S., Kaur, N. and Singh, S. 2009. Photocatalytic degradation of two commercial reactive dyes using nano photocatalysts. *Nanoscale Research Letters*, 4: 709-716.
5. Prabha, I. and Lathasree, S. 2013. Photocatalytic performance of nanocatalyst for the effective removal of dye in the wastewater. *Chemical Science Transactions*, 2(1): 220-224.
6. Ullah, I., Ali, S., Hanif, M. and Shahid, S. 2012. Nanoscience for environmental remediation: A Review. *International Journal of Chemical and Biochemical Sciences*, 2: 60-77.
7. Yuhas, B.D., Smeigh, A.L., Douvalis, A.P., Wasielewski, M.R. and Kanatzidis, M.G. 2012. Photocatalytic Hydrogen evolution from FeMoS-Based biomimetic Chalcogels. *Journal of American Chemical Society*, 134(25): 10353-10356.
8. Lu, X., Zhai, T., Cui, H., Shi, J., Xie, S., Huang, Y., Liang, C. and Tong, Y. 2011. Redox cycles promoting photocatalytic hydrogen evolution of CeO₂ nanorods. *Journals of Material Chemistry*, 21(15): 5569-5572.
9. Zhang, J., Li, L., Huang, X. and Li, G. 2012. Fabrication of Ag-CeO₂ core-shell nanospheres with enhanced catalytic performance due to strengthening of the interfacial interactions. *Journal of Material Chemistry*, 22(21): 10480-10487.
10. Reddy, B.M., Lakshmanan, P. and Khan, A. 2004. Investigation of surface structures of dispersed V₂O₅ on CeO₂-SiO₂, CeO₂-TiO₂ and CeO₂-ZrO₂ mixed oxides by XRD, Raman, and XPS techniques. *Journal of Physical Chemistry B*, 108 (43): 16855-16863.
11. Camino, D., Deroo, D., Salardenne, J. and Treuil, N. 1995. (CeO₂)(TiO₂) 1-x counters electrode materials for lithium electrochromic devices. *Solar Energy Materials and Solar Cells*, 39: 349-366.
12. Yoon, K.H., Cho, J. and Kang, D.H. 1999. Physical and photoelectrochemical properties of the TiO₂/ZnO system. *Materials Research Bulletin*, 34(9): 1451-1461.
13. Reddy, B.M., Khan, A., Lakshmanan, P., Aouine, M., Loridant, S. and Volta, J.C. 2005. Structural characterization of nanosized CeO₂-SiO₂, CeO₂-TiO₂, and CeO₂-ZrO₂ catalysts by XRD, Raman, and HREM techniques. *Journal of Physical Chemistry B*, 109 (8): 3355-3363.
14. Song, Y., Zhao, H., Chen, Z., Wang, W., Huang, L., Xu, H. and Li, H. 2016. The CeO₂/Ag₃PO₄ photocatalyst with stability and high photocatalytic activity under visible light irradiation. *Physical Status Solidi A*, 213(9): 2356-2363.
15. You, D.T., Pan, B., Jiang, F., Zhou, Y.G. and Su, W.Y. 2016. CdS nanoparticles/CeO₂ nanorods composite with high-efficiency visible-light-driven photocatalytic activity. *Applied Surface Science*, 363: 154-160.
16. Gogoi, A. and Sarma, C.K. 2017. Synthesis of the novel β-cyclodextrin supported CeO₂ nanoparticles for the catalytic degradation of methylene blue in aqueous suspension. *Materials Chemistry and Physics*, 194: 327-336.
17. Abi M. Taddesse., Tigabu Bekele., Isabel Diaz. and Abebaw Adgo. 2021. Polyaniline supported CdS/CeO₂/Ag₃PO₄ nanocomposite: An "A-B" type tandem n-n heterojunctions with enhanced

- photocatalytic activity. *Journal of Photochemistry and Photobiology, A: Chemistry*, 406: 113005.
18. Singh, V., Sharma, P. and Chauhan, P. 2011. Synthesis of CdS nanoparticles with enhanced optical properties. *Material Characterization*, 62(1): 43-52.
 19. Ijaz, S., Ehsan, M.F., Ashiq, M.N., Karamat, N. and He, T. 2016. Preparation of CdS/CeO₂ core/shell composite for photocatalytic reduction of CO₂ under visible-light irradiation. *Applied Surface Science*, 390: 550-559
 20. Hong, R.Y., Li, J.H., Chen, L.L., Liu, D.Q., Li, H.Z., Zheng, Y. and Ding, J. 2009. Synthesis, surface modification and photocatalytic property of ZnO nanoparticles. *Journal of Powder Technology*, 189: 426-432.
 21. Liu, B., Zhao, X., Terashima, C., Fujishima, A. and Nakata, K. 2014. Thermodynamic and kinetic analysis of heterogeneous photocatalysis for semiconductor systems. *Physical Chemistry Chemical Physics*, 16: 8751-8760.
 22. Saggiaro, E.M., Oliveira, A.S., Pavesi, T., Maia, C.G., Ferreira, L.F.V. and Moreira, J.C. 2011. Use of titanium dioxide photocatalysis on the remediation of model textile wastewaters containing Azo dyes. *Molecules*, 16: 10370-10386.
 23. Leng, Y. 2008. *Materials characterization: Introduction to microscopic and spectroscopic methods*, John Wiley and Sons (Asia) Pte Ltd.
 24. Roggenbuck, J., Schaer, H., Tsoncheva, T., Minchev, C., Hanss, J. and Tiemann, M. 2007. Mesoporous CeO₂: Synthesis by nanocasting, characterization and catalytic properties. *Microporous and Mesoporous Materials*, 101: 335-341.
 25. Hernandez-Gordillo, A., Romero, A.G., Tzompantzi, F. and Gomez, R. 2013. New nanostructured CdS fibers for the photocatalytic reduction of 4-nitrophenol. *Powder Technology*, 250: 97-102.
 26. Zhang, X., Zhang, N., Xu, Y. and Tang, Z.R. 2015. One-dimensional CdS nanowires CeO₂ nanoparticles composites with boosted photocatalytic activity. *New Journal of Chemistry*, 39: 6756-6764.
 27. Banerjee, R., Jayakrishnan, R. and Ayyub, P., 2000. Effect of the size induced structural transformation on the band gap in CdS nanoparticles. *Journal of Physics: Condensed Matter*, 12: 10647-10654.
 28. Gupta, V., Gupta, A.R. and Kant, V. 2013. Synthesis, characterization and biomedical application of nanoparticles. *Science International*, 1(5): 167-174.
 29. Akram, M., Kanwal, Z., Rauf, A., Sabri, N., Riaz, S. and Naseem, S. 2016. Size and shape dependent antibacterial studies of silver nanoparticles synthesized by wet chemical routes. *Nanomaterials*, 6: 74-79.
 30. Shen, Z., Chen, G., Yu, Y., Wang, Q., Zhou, C., Hao, L., Li, Y., He, L. and Mu, R. 2012. Sonochemistry synthesis of nanocrystals embedded in a MoO₃/CdS core-shell photocatalyst with enhanced hydrogen production and photodegradation. *Journal of Material Chemistry*, 22: 19646-19651.
 31. El-Kemary, M., El-shamy, H. and El-mahasseb, I. 2010. Photocatalytic degradation of Ciprofloxacin drug in water using ZnO nanoparticles. *Journal of Luminescence*, 130: 2327-2331.

32. Kubelka, P. and Munk, F. 1931. Use of diffuse reflectance spectroscopy for optical characterization of un-supported nanostructures. *Journal of Applied Physics*, 12: 593-620.
33. Tauc, T. and Abeies, F. 1970. Optical properties of solids. IOP Publishing Ltd, North Holland, Amsterdam, p. 903.
34. Zou, Z., Qiu, Y., Xie, C., Xu, J., Luo, Y., Wang, C. and Yan, H. 2015. CdS/TiO₂ nanocomposite film and its enhanced photoelectric responses to dry air and formaldehyde induced by visible light at room temperature. *Journal of Alloys Compound*, 645: 17-23.
35. Lopez, R. and Gomez, R. 2012. Band-gap energy estimation from diffuse reflectance measurements on sol-gel and commercial TiO₂: a comparative study. *Journal of Sol-Gel Science and Technology*, 61: 1-7.
36. Magesh, G., Viswanathan, B., Viswanath, R. P. and Varadarajan, T. K. 2009. Photocatalytic behavior of CeO₂-TiO₂ system for the degradation of methylene blue. *Indian Journal of Chemicals*, 3: 480-488.
37. Umezawa, N., Shuxin, O. and Ye, J. 2011. Theoretical study of high photocatalytic performance of Ag₃PO₄. *Physical Review*, B. 83: 035202.
38. Dos Santos, M.L., Lima, R.C., Riccardi, C.S., Tranquilin, R.L., Bueno, P.R., Varela, J.A. and Longo, E. 2008. Preparation and characterization of ceria nanospheres by microwave- hydrothermal method. *Materials Letters*, 62: 4509-4511.
39. Zawadzki, M. 2008. Preparation and characterization of ceria nanoparticles by microwave- assisted solvothermal process. *Journal of Alloys Compounds*, 454: 347-351.
40. Khalil, K.M.S., Leena, A., Elkabee, L.A. and Murphy, B. 2005. Preparation and characterization of thermally stable porous ceria aggregates formed via a sol-gel process of ultrasonically dispersed cerium (IV) isopropoxide. *Microporous and Mesoporous Materials*, 78: 83-89.
41. Yu, X., Ye, P., Yang, L., Yang, S., Zhou, P. and Gao, W. 2007. Preparation of hexagonal cerium oxide nanoflakes by a surfactant free route and its optical property. *Journal of Material Research*, 22: 3006-3013.
42. Prekajski, M., Fruth, V., Andronescu, C., Trandafilovic, L.V., Pantic, J., Kremenovic, A. and Matovic, B. 2013. Thermal stability of Ce_{1-x}Bi_xO₂. (x = 0.1-0.5) solid solution. *Journal of Alloys and Compounds*, 578: 26-31.
43. Salimi, F., Abdollahifar, M., Jafari, P. and Hidaryan, M. 2017. A new approach to synthesis and growth of AlOOH nanocrystalline with high pore volume. *Journal of Serbia Chemical Society*, 82: 1-11.
44. Ho, C., Yu, J.C., Kwong, T., Mak, A.C. and Lai, S. 2005. Morphology controllable synthesis of mesoporous CeO₂ nano and microstructures. *Chemical Materials*, 17: 4514-4522.
45. Lefebvre, J., Austing, D.G., Bond, J. and Finnie, P. 2006. Photoluminescence imaging of suspended single-walled carbon nanotubes. *Nano Letters*, 6: 1603-1608.
46. Katsumata, H., Hayashi, T., Taniguchi, M., Suzuki, T. and Kaneco, S. 2014. Highly efficient visible light driven AgBr/Ag₃PO₄ hybrid photocatalysts with enhanced photocatalytic activity. *Materials Science in Semiconductor Processing*, 25: 68-75.

47. Ji, P., Zhang, J., Chen, F. and Anpo, M. 2009. Study of adsorption and degradation of Acid Orange 7 on the surface of CeO₂ under visible light irradiation. *Applied Catalysis B*, 85(3-4), 148-154.
48. Gezahegn Geresu. 2017. Polyaniline supported CdS/ZnO/Ag₃PO₄ nanocomposite: synthesis and characterization for photocatalytic activity and antimicrobial applications. MSc Thesis, Haramaya University, Haramaya, Ethiopia.
49. Zhou, P., Le, Z., Xie, Y., Fang, J. and Xu, J. 2017. Studies on facile synthesis and properties of mesoporous CdS/TiO₂ composite for photocatalysis applications. *Journal of Alloys and Compounds*, 692: 170-177.
50. Ren, J., Chai, Y., Liu, Q., Zhang, L. and Dai, W.L. 2017. Intercorrelated Ag₃PO₄ nanoparticles decorated with graphic carbon nitride: Enhanced stability and photocatalytic activities for water treatment. *Applied Surface Science*, 403: 177-186.
51. Wang, P., Huang, B., Qin, X., Zhang, X., Dai, Y., Wei, J. and Whangbo, M.H. 2008. Ag/AgCl: a highly efficient and stable photocatalyst active under visible light. *Angewandte Chemie International Edition*, 47: 7931-7933.
52. Zhang, W., Hu, C., Zhai, W., Wang, Z., Sun, Y., Chi, F., Ran, S., Liu, X. and Lv, Y. 2016. Novel Ag₃PO₄/CeO₂ p-n hierarchical heterojunction with enhanced photocatalytic performance. *Materials Research*, 19(3): 673-679.
53. Fujishima, A., Rao, T.N. and Tryk, D.K. 2000. Titanium dioxide photocatalysis. *Journal of Photochemistry and Photobiology C: Photochemistry Reviews*, 1(1): 1-21.
54. Hidalgo, D., Bocchini, S., Fontana, M., Saraccob, G. and Hernandez, S. 2015. Green and low-cost synthesis of PANI-TiO₂ nanocomposite mesoporous films for photoelectrochemical water splitting. *Royal Society of Chemistry*, 5: 49429-49438.
55. Ameen, A., Akhtar, M.S., Kim, Y.S., Yang, B. and Shin, H.S. 2011. An effective nanocomposite of polyaniline and ZnO: preparation, characterizations, and its photocatalytic activity. *Colloid Polymer Sciences*, 289: 415-421.
56. Li, J., Zhu, L., Wu, Y., Harima, Y., Zhang, A. and Tang, H. 2006. Green and low-cost synthesis of PANI/TiO₂ nanocomposite mesoporous films for photoelectrochemical water splitting. *Polymer*, 47: 7361-7367.

Figures

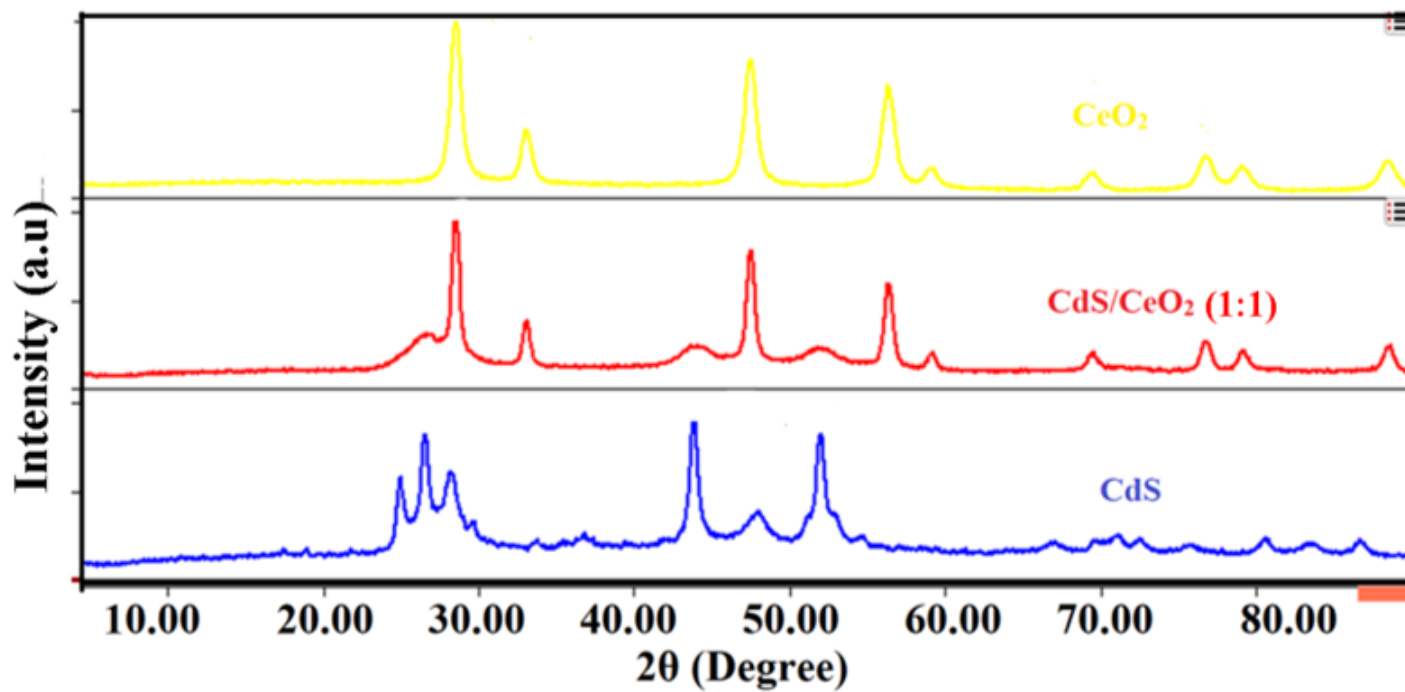


Figure 1

XRD spectra of CeO₂, CdS and CdS/CeO₂ (1:1) photocatalysts

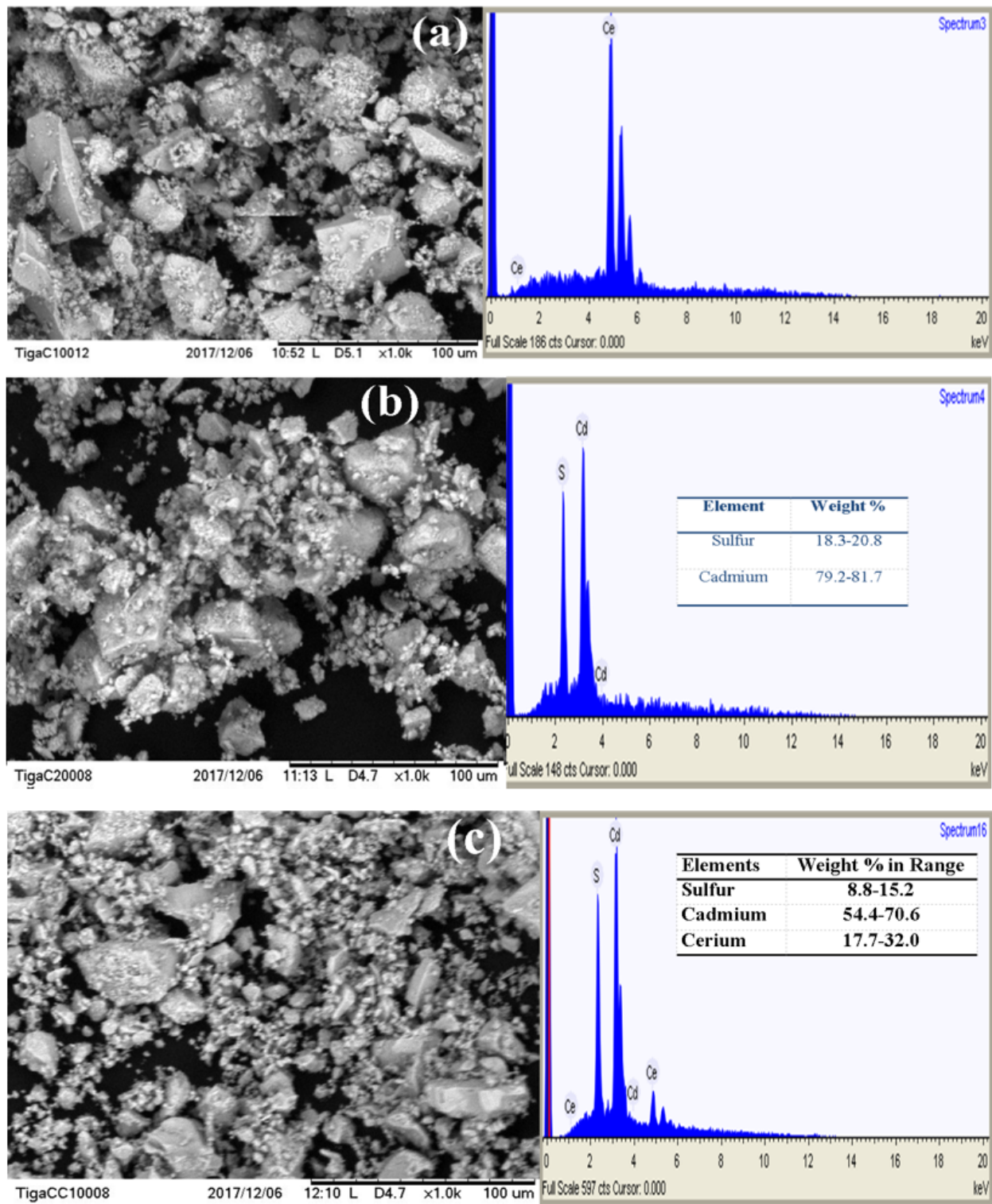


Figure 2

SEM-EDX images of (a) CeO₂, (b) CdS and (c) CdS/CeO₂ (1:1) photocatalyst

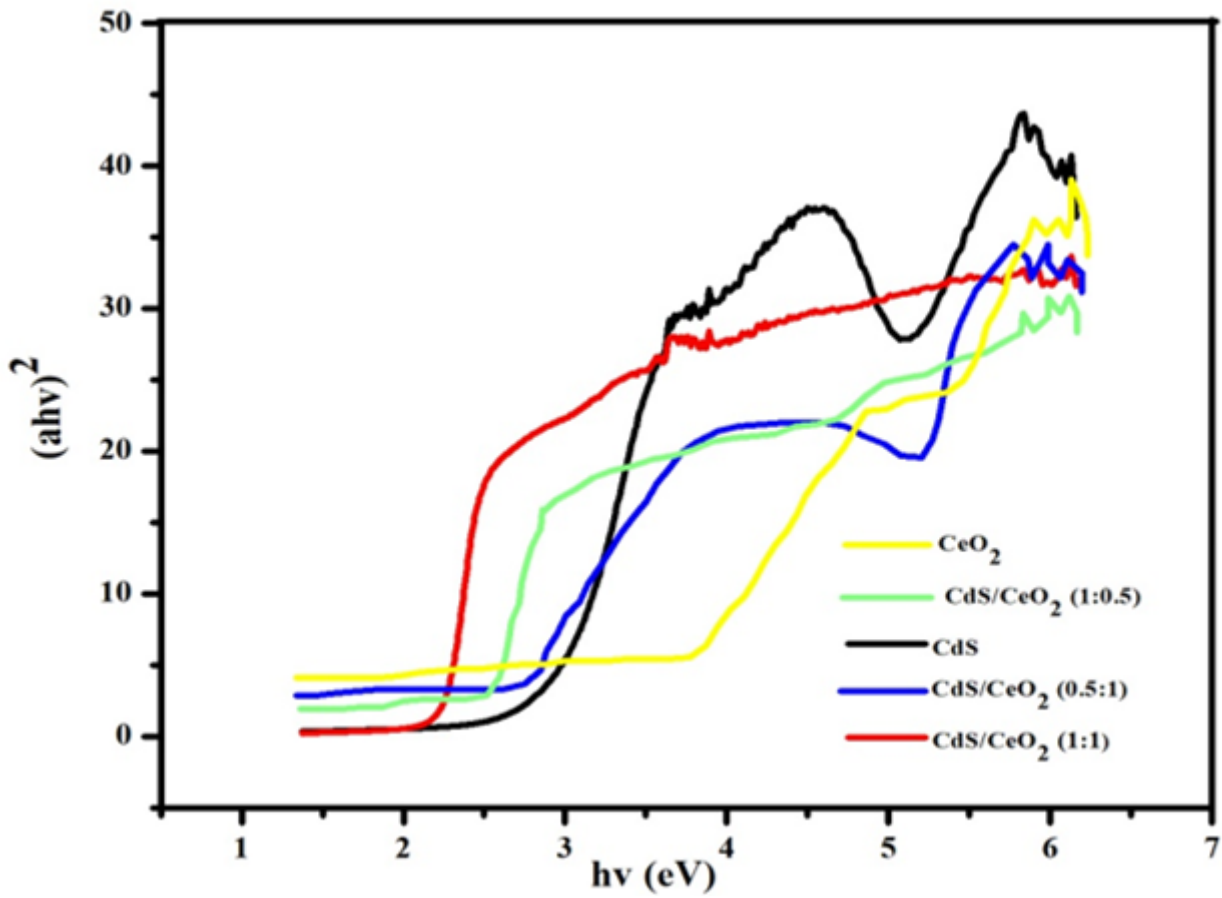


Figure 3

Tauc plot of single (CeO₂ and CdS) and binary CdS/CeO₂ (in different molar ratio) photocatalyst

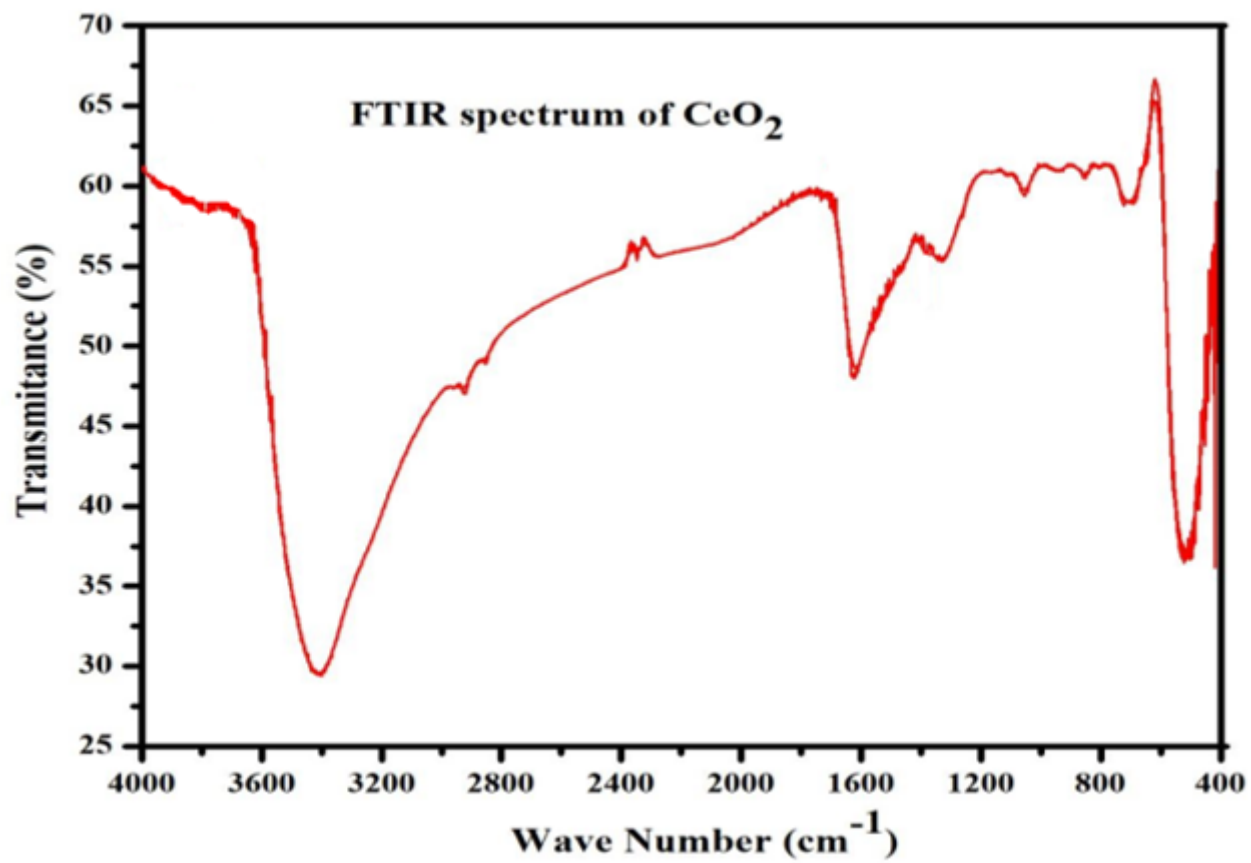


Figure 4

FTIR spectrum of CeO₂ nanoparticle

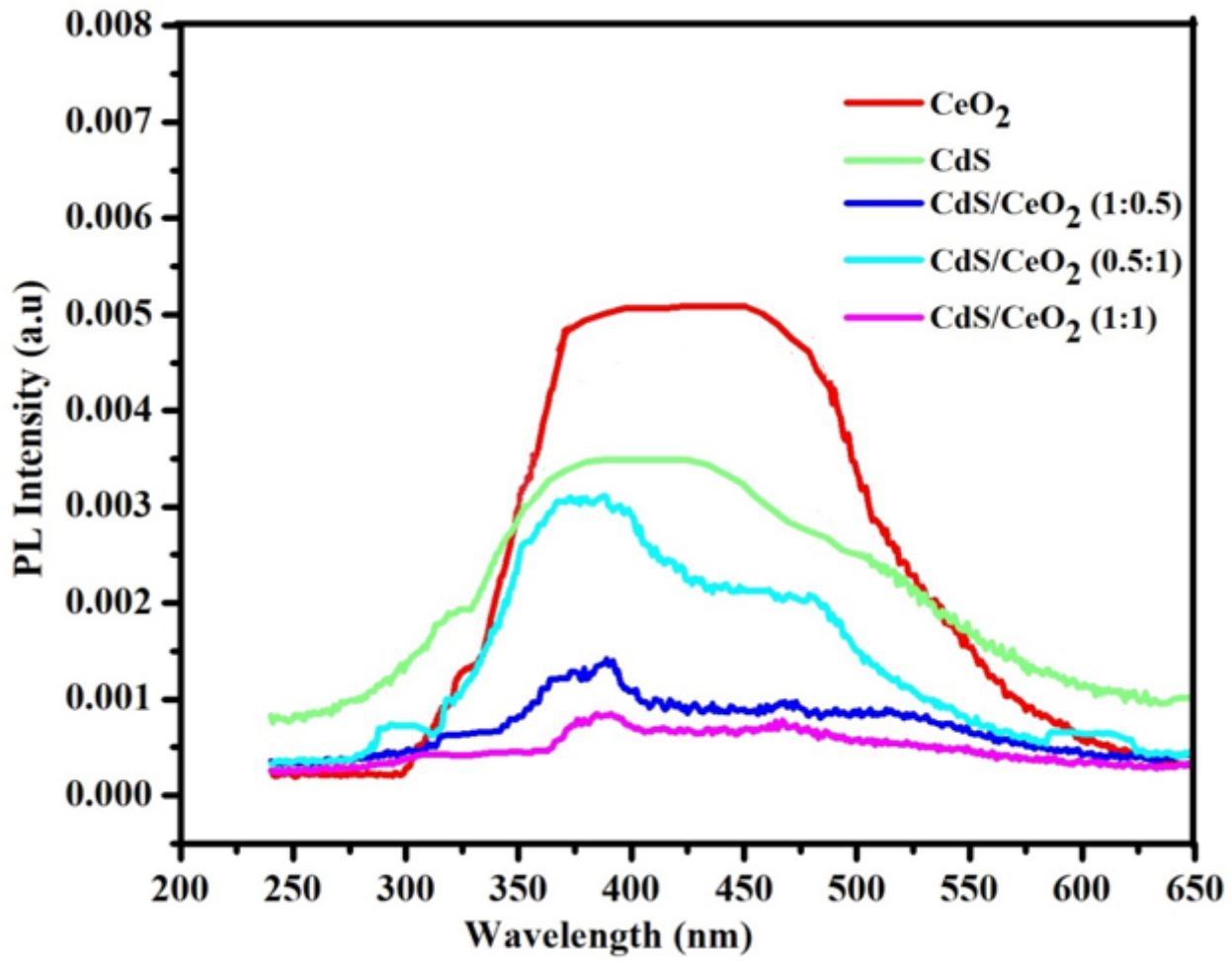


Figure 5

The PL emission spectra of CeO₂, CdS and CdS/CeO₂ (in 0.5:1, 1:1 and 1:0.5 molar ratios) photocatalyst

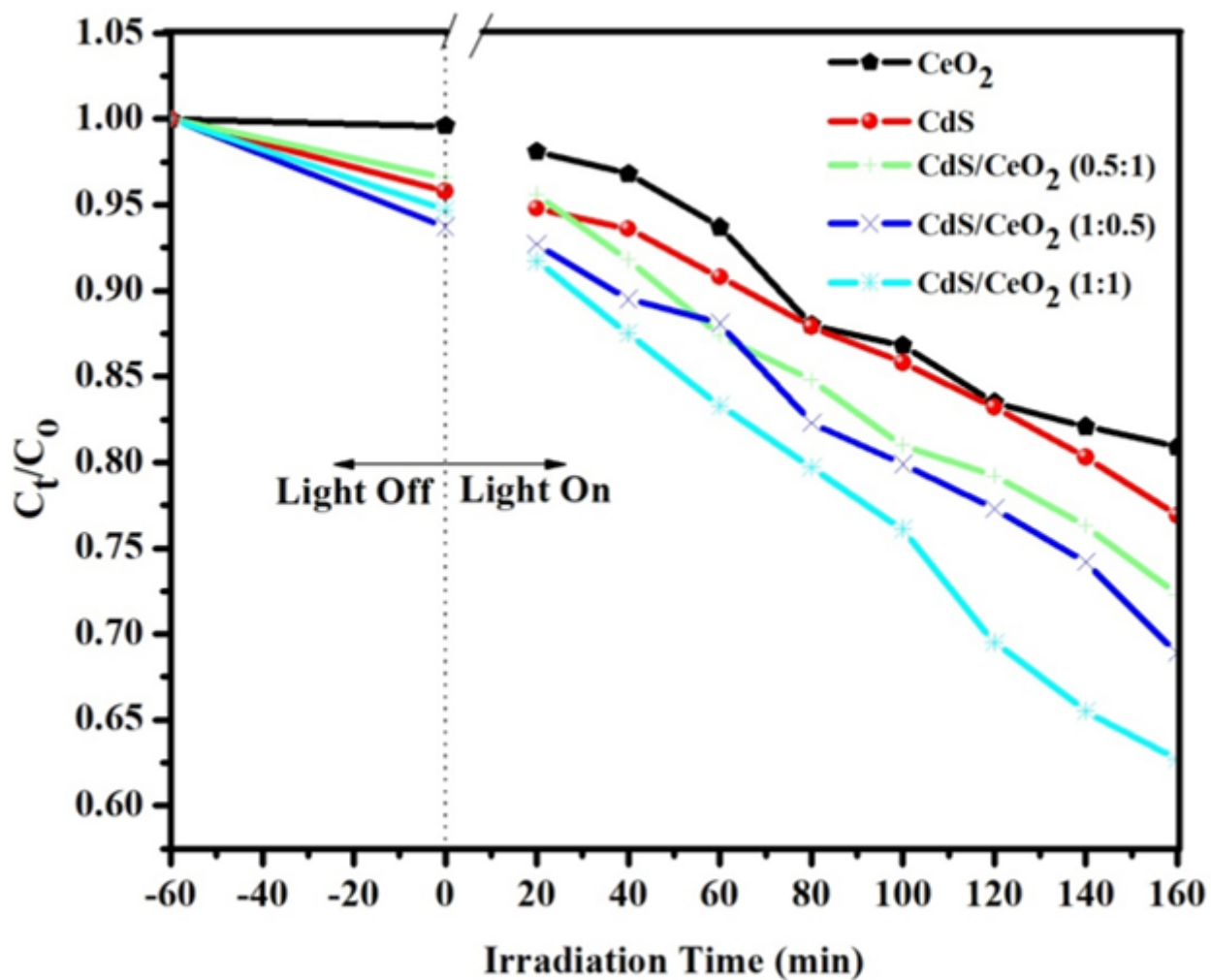


Figure 6

Degradation efficiency of the as-synthesized photocatalyst [CeO₂, CdS, CdS/CeO₂ (in different ratio)] as function of visible irradiation time

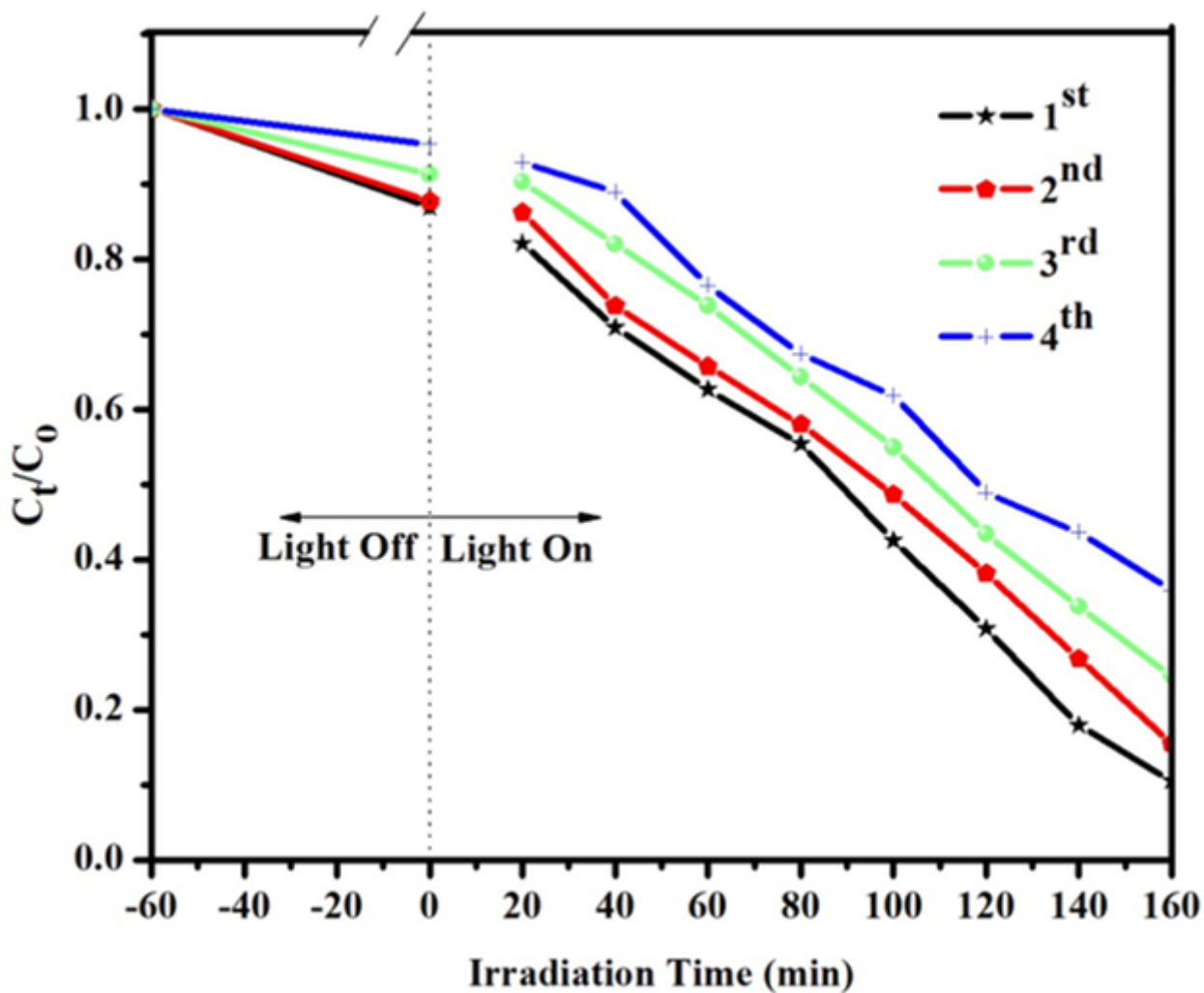


Figure 7

Degradation rate of MeO using CdS/CeO₂ (1:1) photocatalyst as function of irradiation time in different cycles (load at 0.15 g/L, initial concentration of MeO at 10 ppm and pH at 4)

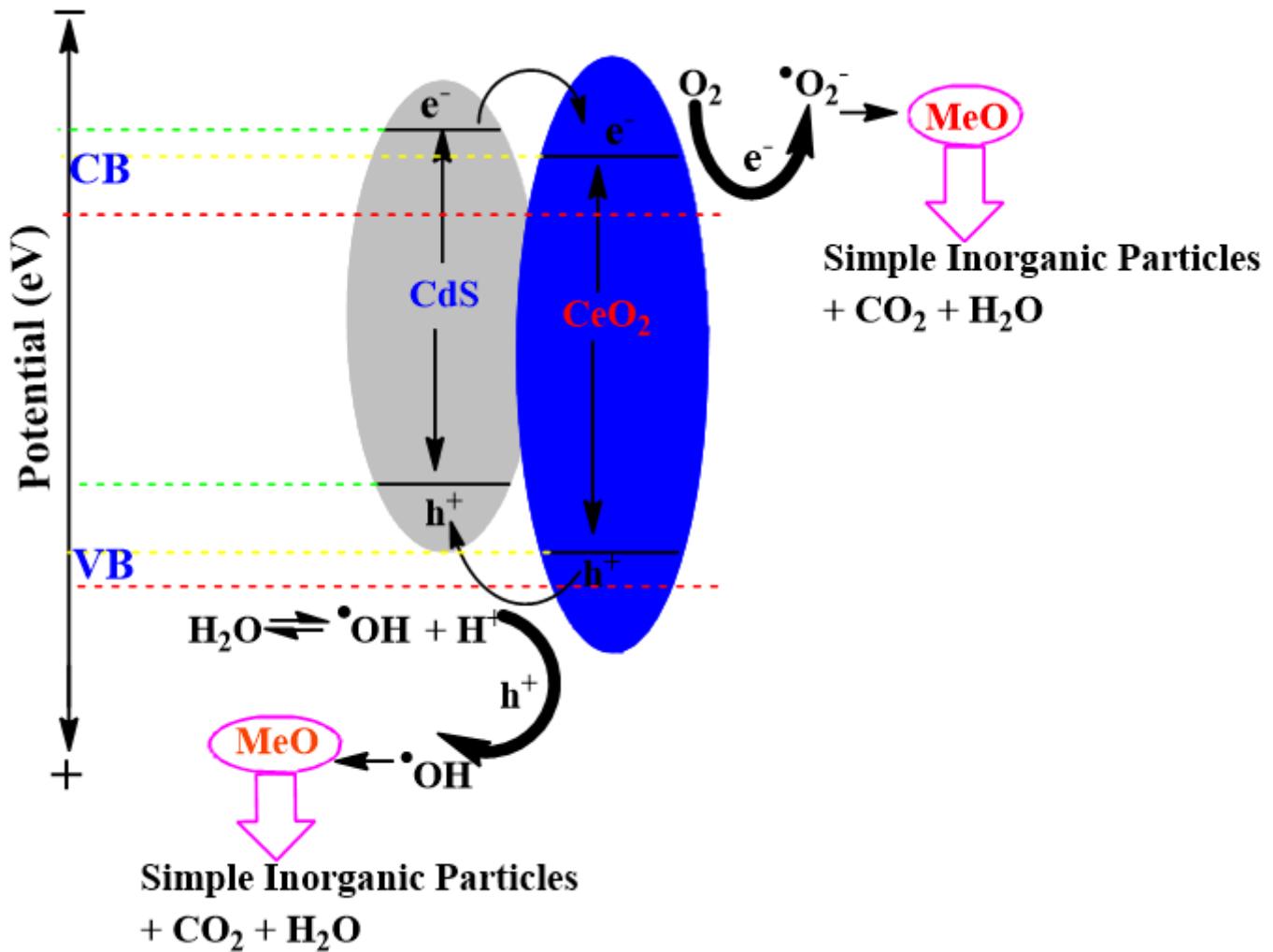


Figure 8

Mechanism of photocatalytic degradation of organic contaminant (MeO) by CdS/CeO₂ photocatalyst under visible light irradiation

Supplementary Files

This is a list of supplementary files associated with this preprint. Click to download.

- [SupportiveAppendixes.png](#)